Stability Enhancement of Admittance Control with Acceleration Feedback and Friction Compensation☆

Myo Thant Sin Aung[a,*], Ryo Kikuuwe[b]

[a] *Department of Mechatronic Engineering, Yangon Technological University, Insein, Yangon, Myanmar*
[b] *Department of Mechanical Engineering, Kyushu University, 744 Motooka, Nishi-ku, Fukuoka 819-0395, Japan*

Abstract

This paper presents an experimental investigation of a new position control scheme that enhances the stability of admittance control by using: (a) PDD^2 (proportional, derivative, and second derivative) feedback, (b) dither-based friction compensation and (c) sliding-mode-based noise filter with a variable gain. The PDD^2 structure and the friction compensation are for expanding the bandwidth of the internal position-controlled subsystem. The sliding-mode-based filter is for the attenuation of noise in the acceleration signal without producing a large phase lag. The variable gain of the filter is for suppressing acceleration-measurement noise at low velocity. The proposed controller is validated by employing a 1-DOF device.

Keywords: Admittance control, Noise filter, Sliding mode, Position control, Overdamped behavior

1. Introduction

For many robotic manipulation tasks, such as force guided assembly, where robots are required to work in contact with the environment or external objects,

☆The paper extends the authors' previous conference publication [1] by including an improved position controller and new experimental results. The difference between the improved position controller and the previous position controller in [1] is explained in Section 3.3, and some experimental comparisons between the two controllers are included in Section 4.

*Corresponding author
Email address: nayaye1@gmail.com (Myo Thant Sin Aung)

appropriate controllers are needed to regulate the contact force between the robot and the environment. There exist many control schemes for force control of robots as surveyed in [2, 3, 4]. Among them, admittance control is a well-suited option when a force sensor is available in the end-effector because the effects of the nonlinearities such as joint friction are suppressed by the internal position controller of the admittance controller.

The block diagram of a common implementation of admittance control is illustrated in Fig. 1. In this control scheme, the motion of a virtual object with simple dynamics is generated from the measured force and an input (desired) force. The robot tracks the virtual object's position under the internal position controller. In this framework, one requires an accurate position controller so that the robot's response to external forces is sufficiently close to that of the virtual object. Admittance control has been implemented in many robotic tasks, e.g., rehabilitation [5, 6], haptic rendering [7], human-robot cooperation [8], and robotic surgery [9].

As noted in [10, 11], a primary source of the instability of admittance control is the limited bandwidth of the internal position controller. In order to enhance the stability, the virtual mass can be set as high as the device mass [12, 13] at the cost of the system being less responsive.

Several previous research works have shown that the use of acceleration signal is effective in expanding the bandwidth of force control systems. Morbi et al. [5] proposed acceleration-limited proportional derivative controller to enhance the stability of admittance control. Xu et al. [14, 15] showed that the joint acceleration feedback by using an accelerometer damps out the oscillations substantially in explicit force control. One of the authors [16] employed a feedforward term of the desired acceleration in combination with a sliding mode-like position controller in admittance control. Aguirre-Ollinger et al. [17] showed that acceleration feedback by using an accelerometer extends the bandwidth of admittance control.

Other approaches that enhances the stability of admittance and impedance controllers have been proposed. Duchaine and Gosselin [18] implemented vari-

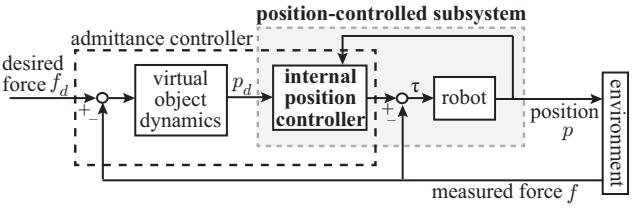

Figure 1: Block diagram of an admittance-controlled robot in contact with an environment.

able damping to enhance the stability of admittance control. Hashimoto et al. [19] applied a nonlinear admittance controller in which the stiffness is varied according to the displacement of the leg in a biped robot. By using an adaptive controller, Tee et al. [20] proposed a variable admittance control scheme to deal with unmodeled dynamics. Osa et al. [21] proposed a hybrid controller that switches between rate control and admittance control for use in bilateral operations. Dimeas et al. [22] implemented an online learning controller with neural network backpropagation training in the inner loop of the admittance controller. An interaction controller that combines friction compensation and disturbance observer was proposed in [23].

Our preliminary work [1] investigated the use of acceleration feedback and friction compensation in the position control loop for enhancing the stability of admittance control. In this paper, we propose a new position controller that produces better force control performance by allowing higher acceleration feedback gain than our previous controller [1]. The proposed control scheme comprises three components: (a) PDD^2 (proportional, derivative, and second derivative) position controller, (b) dither-based friction compensator [24] and (c) sliding-mode-based noise filter with a variable gain. The D^2 term is used to enhance the stability because its phase-lead effect theoretically extends the bandwidth of the position-controlled subsystem, i.e., the subsystem with the input p_d and the output p indicated in Fig. 1. The friction compensator proposed by the authors [24] is also used to extend the bandwidth of the position-controlled subsystem by reducing the phase lag caused by the hardware. The sliding-mode-based filter, which is also the one presented by the authors [25], is employed to smooth

the acceleration (second-derivative) signal from the optical encoder without producing a large phase lag. The effect of the noise at low velocity is mitigated by setting the filter gain low when the velocity is low. Experimental results show that the proposed position controller enhances the stability of admittance control.

The present research is distinct from previous works mainly in that it does not require accelerometers, in contrast to [14, 15, 17], or the acceleration estimation based on precalibrated joint's dynamics, in contrast to [5]. In addition, the acceleration feedback presented in this paper can be readily combined with conventional PD or PID position controllers in any admittance control scheme.

The rest of this paper is organized as follows. Section II discusses the theoretical necessity of the second order controller and friction compensation in the new position controller. Section III proposes the new controller. Section IV shows its effectiveness through experimental results and Section V provides some concluding remarks.

2. Preliminary Analysis

2.1. One-DOF System

Here, we discuss the motivation of the new position controller based on an analysis on a one-dimensional robot under admittance control in contact with an environment. The block diagram of such a system is shown in Fig. 1.

A typical admittance-controlled robot with the desired force input f_d comprises a virtual object motion generator and a position servo for controlling the robot to track the motion of the virtual object. A common type of such a controller can be described as follows:

$$\ddot{p}_d = \frac{-b\dot{p}_d - f + f_d}{m} \tag{1a}$$

$$\tau = K(p_d - p) + B(\dot{p}_d - \dot{p}). \tag{1b}$$

Here, f denotes the measured external force, the desired force f_d and the measured position p are the inputs to the controller while τ is the torque command

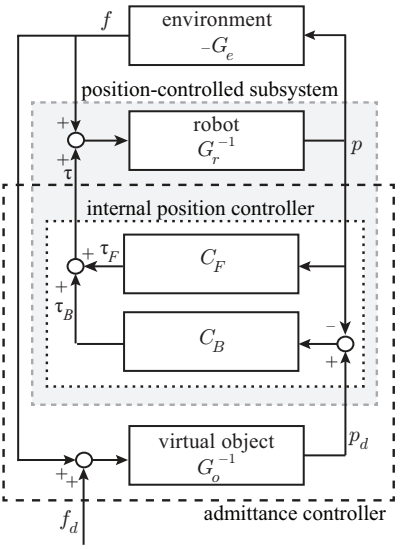

Figure 2: Detailed block diagram of the system of Fig. 1.

sent to the actuator. The virtual object dynamics is modeled as in (1a), where the constants m and b represents the inertia and the viscosity of the object. One can regard (1a) as a controller to make the measured force f track the desired value f_d, where the virtual object position p_d is the desired input to the internal position controller, of which K and B are P-, and D-gains, respectively.

2.2. Phase Lag and Instability

The analysis in this section follows a similar path to the analysis in [26], where a bilateral master-slave system is analyzed. Figure 2 is a more detailed block diagram of the system of Fig. 1. Hereafter, all symbols are defined in the Laplace transform domain and are functions of the Laplace operator s. In Fig. 2, G_o is the dynamics of the virtual object, C_B and C_F are the components of the position controller, G_r is the dynamics of the robot and G_e is the dynamics of the environment. We describe the dynamics of the virtual object as follows:

$$G_o p_d = f_d + f. \tag{2}$$

We also assume that the robot is a single mass and its dynamics can be described as follows:

$$G_r p = \tau + f \tag{3}$$

where p is the position of the robot. Two forces, the actuator force τ and the contact force f, are acting on the robot. The position controller is described as follows:

$$\tau = C_B(p_d - p) + C_F p \tag{4}$$

where C_B denotes the transfer function of the position controller and C_F corresponds to a compensator that partially compensates the dynamics of the robot. In this paper, C_F is considered as the friction compensator. The contact with the environment can be modeled as follows:

$$f = -G_e p \tag{5}$$

where G_e is the dynamics of the environment. From (2), (3) and (4), the followings are obtained:

$$p = U_C p_d + \frac{1}{G_r - C_F + C_B} f \tag{6}$$

$$p = Z_s f + \frac{U_C}{G_o} f_d \tag{7}$$

where

$$U_C \triangleq \frac{C_B}{G_r - C_F + C_B} \tag{8}$$

$$Z_s \triangleq \frac{U_C}{G_o} + \frac{1}{G_r - C_F + C_B}. \tag{9}$$

Equation (6) indicates that U_C can be understood as the transfer function of the position-controlled subsystem. Equation (7) describes the response of the end-effector position p according to the force f applied to the end-effector and the desired force f_d provided to the controller.

The open-loop relation (7) is closed by the end-effector's contact with an environment, which constitutes the feedback loop (5) from the end-effector position p to the force f. The 'feedback' gain $|G_e|$ can be high during the contact

with a stiff environment. Due to the Nyquist stability criterion, the closed-loop system may become unstable with a high $|G_e|$ if there is a frequency range at which $\angle Z_s \leq -\pi$ holds true. In the definition of Z_s in (9), the denominators G_o and $G_r - C_F + C_B$ are polynomials of at most the second order. Therefore, if $U_C = 1$ is satisfied, i.e., if the bandwidth of the position-controlled subsystem is infinite, $\angle Z_s > -\pi$ is always satisfied. Due to the definition (8) of U_C, however, $U_C = 1$ cannot hold true. This means that the admittance-controlled robot can become unstable due to the phase lag caused by U_C especially when the robot is in contact with a stiff environment.

In order to reduce the phase lag caused by the position-controlled subsystem U_C, one needs to make U_C as close as possible to 1 and it can be done by appropriate settings of C_B and C_F. The controller C_B should be set so that $|C_B|$ is as high as possible at least in comparison to $|G_r - C_F|$ in a wide range of the frequency domain. The compensator C_F should be chosen so that $|G_r - C_F|$ is sufficiently small while maintaining the stability of the transfer function $G_r - C_F$. For these reasons, one can conclude that the controller C_B should be a polynomial of the second order, instead of the first order, and that the compensator C_F should be carefully chosen based on the precalibrated parameters of G_r. The controller C_B of the second order corresponds to a PDD^2 position controller. If the position control gains are infinitely high ($|C_B| = \infty$), the definitions (8) and (9) of U_C and Z_s reduce to $U_C \approx 1$ and $Z_s \approx 1/G_o$, respectively, and also the relation (7) becomes close to the following:

$$p = \frac{1}{G_o}(f + f_d). \tag{10}$$

This is exactly the ideal admittance control with which the designed virtual object dynamics is realized by the relation between the position p and the force $f + f_d$. Thus, one can say that using a high-gain PDD^2 position controller and an appropriate compensator C_F has positive effects both on the stability and on the accuracy of the admittance control.

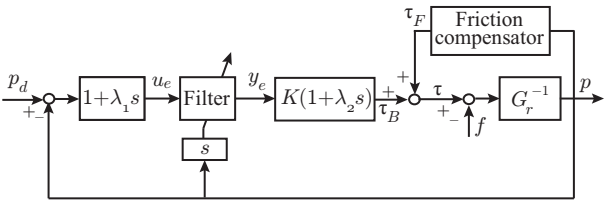

Figure 3: Block diagram of the proposed controller.

3. New Position Controller

Being motivated by the analysis in the previous section, this section presents a position controller for realizing a better stability of admittance control. The proposed position controller comprises the following three features:

(a) PDD^2 error feedback

(b) friction compensator [24]

(c) sliding-mode-based filter [27] with a variable gain.

Figure 3 shows the overall structure of the proposed controller. The PDD^2 error feedback corresponds to the block C_B in Fig. 2, and its effect can be theoretically justified as in the previous section. The friction compensator, which is detailed in [24], is to reduce the effect of friction. It corresponds to the block C_F in Fig. 2. The sliding-mode-based filter is the one proposed in [25], which has been shown to be effective in noise attenuation without producing large phase lag. As a new feature proposed in this paper, the filter gain is set lower when the noise is high. This section explains these features.

3.1. PDD^2 Controller

The input to the PDD^2 controller is the positional error $p_d - p$ and the output is as follows:

$$\tau_B = K(p_d - p) + K(\lambda_1 + \lambda_2)(\dot{p}_d - \dot{p}) + K\lambda_1\lambda_2(\ddot{p}_d - \ddot{p}) \tag{11}$$

where K, λ_1 and λ_2 are positive constants. The structure of (11) implies that the zeros of the transfer function C_B are set to be on the real axis so that the

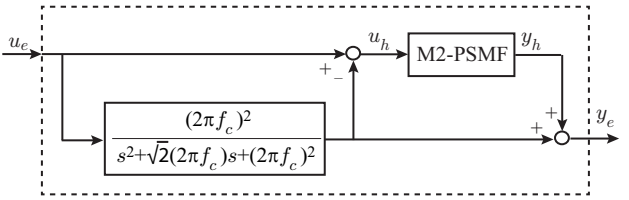

Figure 4: Block diagram of the sliding-mode-based filter proposed in [25]. Here, f_c is the cut-off frequency of the second-order linear low-pass filter (2-LPF) in hertz.

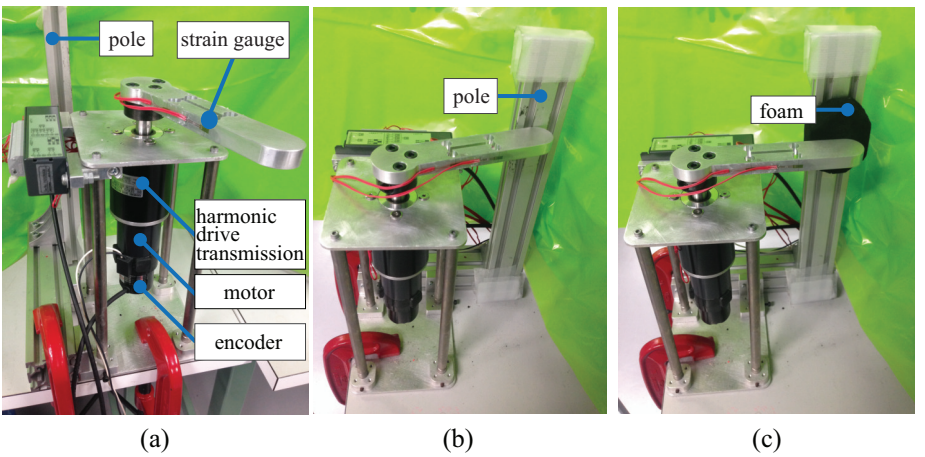

Figure 5: (a) Experimental setup. (b) Contact with aluminum pole. (c) Contact with foam sheet.

response is overdamped when the gain K is sufficiently high. The controller (11) performs the PD-type action of $K(1+\lambda_2 s)$ on a phase-led positional error signal through the phase lead compensator $(1+\lambda_1 s)$, and thus, it can also be viewed as a phase-led PD controller.

3.2. Friction Compensator

The proposed positional controller employs the encoder-based friction compensator presented by the authors [24]. Its details can be found in [24]. The compensator accepts the encoder signal p as its input, and provides the force τ_F in Fig. 3 as its output. When the velocity $\dot{p}$ is small, the compensator provides a dither signal in order to maintain the controlled object on the verge of the

static friction state, and thus, the system becomes sensitive to external forces. Once the velocity is large, the compensator cancels the friction force based on a precalibrated rate-dependent friction law.

3.3. Variable Gain Sliding-mode-based Filter

It is easy to infer that the use of the PDD^2 controller (11) produces the noisy output due to the derivative action on the encoder signal. The noise may be attenuated by some noise filters but, usually, filters cause phase lag between the input and the output. To attenuate noise without producing large phase lag, a sliding-mode-based filter, which is the one presented by the authors [25], was used in [1]. It produces smaller phase lag than a second order low-pass filter and other sliding mode filters such as those presented in [28] and [29]. It is composed of the sliding mode filter called M2-PSMF and the second order Butterworth low-pass filter (2-LPF). Its block diagram is shown in Fig. 4, where u_e is the input and y_e is the output. The continuous-time representation of M2-PSMF is as follows:

$$\dot{x}_1 = x_2 \tag{12a}$$

$$\dot{x}_2 \in -\frac{H+1}{2} F \mathrm{sgn}(2F(x_1 - u_h) + |x_2|x_2) - \frac{H-1}{2} F \mathrm{sgn}(x_2 - \dot{u}_h) \tag{12b}$$

$$y_h = x_1 \tag{12c}$$

where $H > 1$ and $F > 0$ are parameters appropriately chosen.

It was reported in [1] and [27] that, in the low velocity region, the filter (12) failed to attenuate the noise attributed to the use of large value of λ_1. Moreover, in our case, the friction compensator produces dither signal when the velocity is very low. To reduce the problem of the noise in such cases, we proposed in [1] to set the coefficient λ_1 low when the velocity is lower than a particular threshold, which is described as follows:

$$\lambda_1(\dot{p}) \triangleq \begin{cases} \lambda_{1H} & \text{if } |\dot{p}| \geq v_s \\ \lambda_{1L} & \text{otherwise} \end{cases} \tag{13}$$

where λ_{1H}, λ_{1L} and v_s are appropriately selected positive parameters that satisfy $\lambda_{1H} > \lambda_{1L}$.

In this paper, a new approach is proposed where the gain of the filter (12) is varied according to the velocity. Specifically, the gain F is determined as the following function of the velocity $\dot{p}$:

$$F(\dot{p}) \triangleq \begin{cases} F_H & \text{if } |\dot{p}| \geq v_s \\ F_L & \text{otherwise} \end{cases} \tag{14}$$

where F_H and F_L are appropriately selected positive parameters that satisfy $F_H > F_L$. The objective of (14) is to allow the use of high value of λ_1, which is advantageous in both extending the bandwidth and enhancing the disturbance rejection of the position-controlled subsystem as reported in [27]. The level of amplified noise due to second derivative is reduced by setting F low when the velocity is lower than the threshold v_s.

4. Experiments

4.1. Setup

This section presents the experimental validation of the proposed controller. Experiments were conducted by using a single link robotic joint shown in Fig. 5(a), which comprises of a DC servo motor integrated with a harmonic drive transmission and an incremental optical encoder. The gear ratio of the transmission was 100 and the resolution of the encoder was 9.0×10^{-4} deg per count in the output shaft of the transmission. The control system was implemented with a PC running the ART-Linux operating system. Four strain gauges, with the gauge factors of approximately 2, connected in a Wheatstone bridge configuration, are used to measure the force acting on the link.

The most destabilizing task in admittance control is the contact force control with the rigid environment. To validate the performance of the proposed controller in both rigid and soft environments, the experimental setup consists of an aluminum pole fixed to the base of the setup, as shown in Fig. 5(a). The

link was controlled to make contact with the aluminum pole [see Fig. 5(b)] or a foam sheet attached to the pole [see Fig. 5(c)]. In addition to the case of contact force control, an example of physical human-robot interactive experiment will also be reported, in which the robot moves following the force applied by the human grasping the link.

In the experiments, the discrete-time implementation of the admittance controller was accomplished by using the backward Euler method and implemented with the time-step size T =0.001 s. The length of the link L was $L = 0.12$ m. The admittance control was performed in the translational system along the circular path of the radius L. In the controller, numerical integration of the virtual object dynamics (1a) was implemented as follows:

$$v_d(k) := (bv_d(k-1) - T(f(k) - f_d(k)))/(mT + b) \tag{15a}$$

$$p_d(k) := p_d(k-1) + Tv_d(k) \tag{15b}$$

where k is the discrete time index. The parameters were chosen as $b = 0.1$ Ns/m and $m = 0.5$ kg for the aluminum pole, and $m = 0.05$ kg for the foam sheet. These values were set as low as the proposed position controller achieves stability for each environment. The position control was performed in the rotational system to track the angle correspondent to the position p_d.

The D^2 term, the variable-gain filter and the friction compensator are the three main features of the proposed position control scheme. Thus, the following schemes were compared in the experiments:

- PDD^2+VFL+FC: the proposed controller, i.e., the combination of PDD^2 controller (11), the variable-gain filter (12)(14), and the friction compensator.
- PDD^2+VFL: the proposed controller without friction compensator, i.e., the PDD^2 controller (11) and the variable-gain filter (12)(14).
- VPDD^2+FL+FC: the controller proposed in [1], i.e., the variable-gain PDD^2 controller (11)(13) combined with the filter (12), and the friction compensator.

- PD: the PD controller, i.e., (11) with $\lambda_1 = 0$ s.

The D^2 action and the friction compensation are expected to produce high-frequency torque command that theoretically results in better stability and better tracking performance. The comparison between PD and PDD^2+VFL is for observing the effects of D^2 term, while the comparison between PDD^2+VFL+FC and PDD^2+VFL is for observing the effects of the friction compensator. The comparison between PDD^2+VFL+FC and VPDD^2+FL+FC is for observing for the advantage of the variable-gain filter (the proposed approach) over the variable-gain PDD^2 (the previous approach [1]). It is expected to provide a better balance between the tracking performance of the contact force and the noisiness of the actuator torque.

Other possible internal position controllers such as PD+FC and VPDD^2+FL have been reported in our previous paper [1] and thus they are not considered in this paper. The bandwidth of the position-controlled subsystem achieved by different controllers may be of some academic interest but here we focus only on the stability and the performance of the whole admittance-controlled system, which is practically much more important.

The parameters $\{K, \lambda_2\}$ were chosen as $K = 30$ Nm/deg, and $\lambda_2 = 0.06$ s. The parameters $\{v_s, f_c, H\}$ were chosen as $v_s = 6$ deg/s, $f_c = 10$ Hz and $H = 3$. The velocity threshold v_s was chosen according to the velocity produced under the dither actuation. The cutoff frequency f_c was chosen by trial and error. The parameter H was set as $H = 3$ according to the guidelines presented in [28]. The parameters of the friction compensator were set the same as in [24]. For the proposed controller (PDD^2+VFL+FC) and PDD^2+VFL, the parameter λ_1 was tuned to achieve stable interaction in the experiments and chosen as $\lambda_1 = 0.01$ s while the parameters $\{F_L, F_H\}$ were tuned so that noisy actuation is avoided and chosen as: $\{F_L = 6000$ deg/s^{-2}, $F_H = 12000$ deg/s$^{-2}\}$. For the controllers VPDD^2+FL+FC and VPDD^2+FL, λ_{1H} is chosen the same as λ_1 and $\lambda_{1L} = 0$ s while F is set the same as F_H.

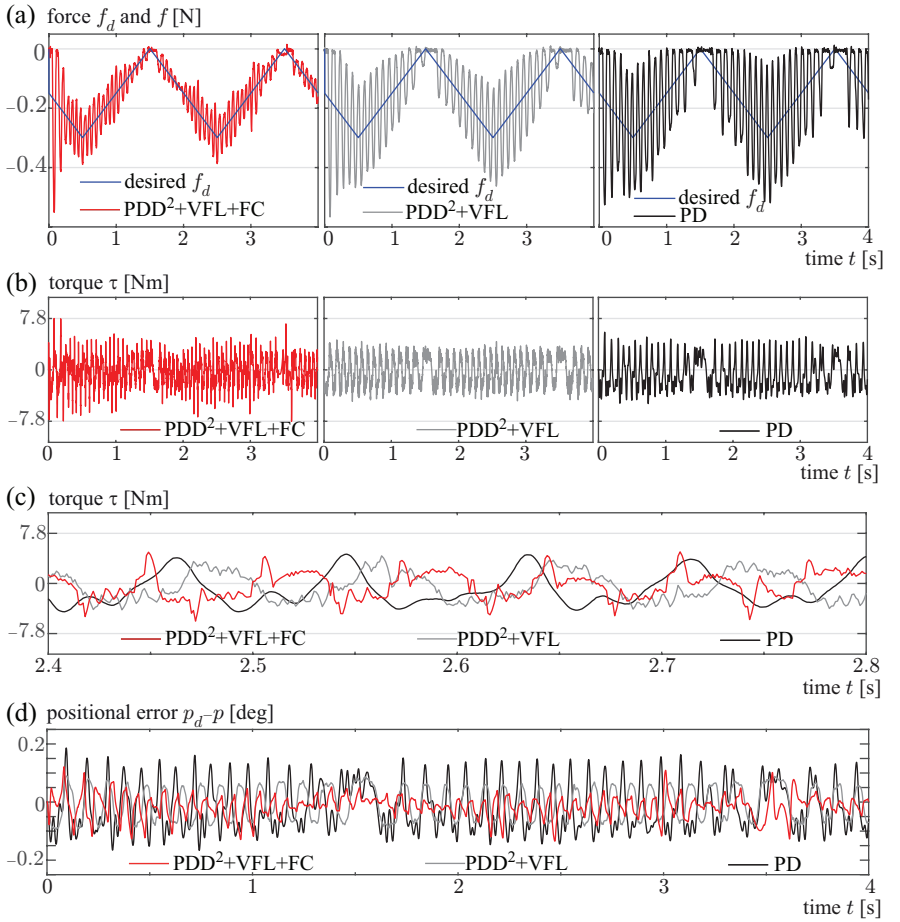

Figure 6: Results of Experiment I: contact force control on the foam sheet.

4.2. Experiment I: Contact Force Control

This section presents a set of experiments to show the effect of the proposed controller in maintaining contact with the environment with varying contact force. The link was initially set about 0.01 m away from the environment before the admittance controller was initiated. The desired force trajectory was chosen as a triangular wave between 0 N and −0.3 N at a frequency of 0.5 Hz.

The results obtained with the soft environment are shown in Fig. 6. It can be seen in Fig. 6(a) that PDD^2+VFL+FC (the proposed controller) achieved better tracking of the contact force f, with smaller oscillation, with respect to the

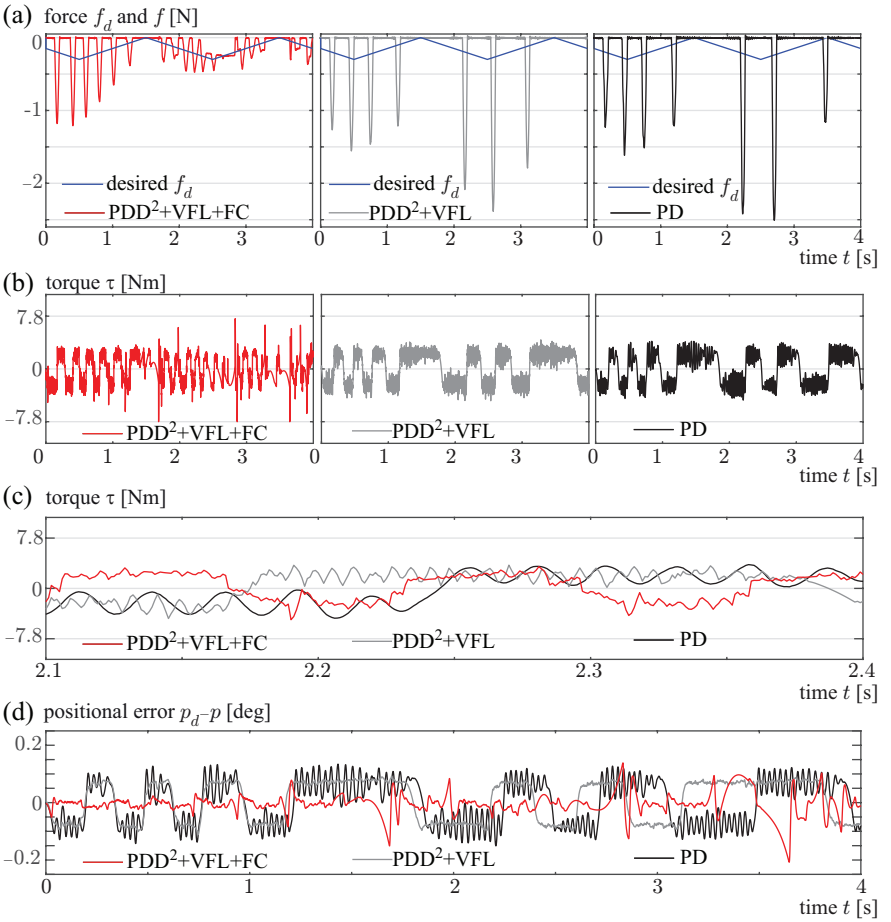

Figure 7: Results of Experiment I: contact force control on the aluminum pole.

desired force f_d than both PDD^2+VFL and PD. Figure 6(b) shows the controller output torques of each controller while Fig. 6(c) shows the detailed view of the output torques. From these figures, one can see that PD produces slowly varying signal while the other two controllers produce more rapidly varying signals. This feature is attributed to the D^2 action and the friction compensator, especially with the dither signal around the zero velocity. The better control performance of PDD^{2}VFL+FC and PDD^2+VFL can be attributed to this rapid, responsive actuation. The graphs in Fig.6(d) show that the error between p_d and p is smallest with the proposed controller (PDD^2+VFL+FC). This feature implies

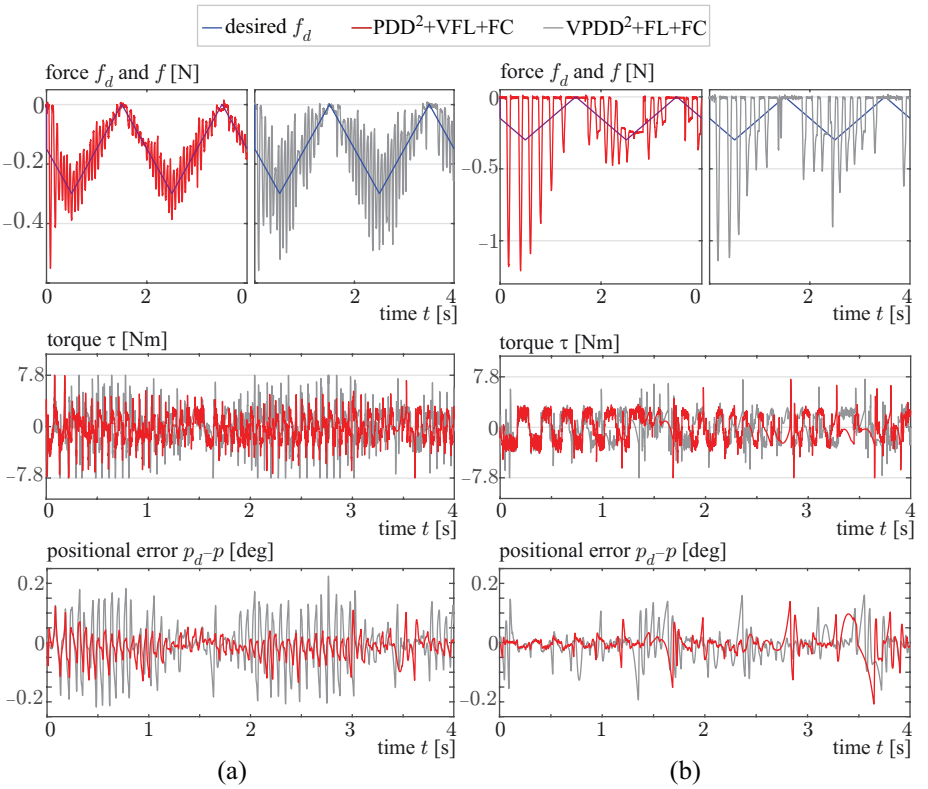

Figure 8: Results of Experiment II for comparison of the proposed controller and the controller in [1]: (a) contact force control on the foam sheet. (b) contact force control on the aluminum pole.

that the performance of the internal position controller is strongly related to the performance of the force control, as suggested by the theoretical analysis in Section 2.

The results obtained with the rigid environment, which is the most destabilizing task in the case of contact force control, are shown in Fig. 7. As is the case with the soft environment, PDD^2+VFL+FC (the proposed controller) outperforms both PDD^2+VFL and PD as shown in Fig. 7(a). This figure also shows the same tendency as the results of the soft environment. Because the environment is much harder, the behavior is less stable and more bouncing than the case of Fig. 6. One can see that, however, the proposed controller

(PDD^2+VFL+FC) produces the smallest bouncing and best accuracy among the three controllers. The controller output torques are shown in Fig. 7(b) and (c), and the positional error is shown in Fig. 7(d). The results in these graphs indicate that the rapid, responsive actuation of the proposed controller produced the best tracking of the contact force among the three controllers and it is also reflected in the positioning error.

The proposed controller was also compared with the previous controller [1] to show the advantage of the variable-gain filter over the variable-gain PDD^2 feedback. The acceleration feedback gain in the proposed controller is kept constant while it is varied in the previous controller [1]. The results of the soft and rigid environments are shown in Fig. 8(a) and (b) respectively. By observing the force signals, it can be seen that PDD^2+VFL+FC (the proposed controller) achieved better performance than VPDD^2+FL+FC (the previous controller [1]) during the contact with both environments. By observing the controller output torque signals, it can be seen that PDD^2+VFL+FC (the proposed controller) produced less noisy actuation, especially during the contact with the soft environment, than VPDD^2+FL+FC (the previous controller [1]). The graphs of positional error show that PDD^2+VFL+FC (the proposed controller) achieved smaller than VPDD^2+FL+FC (the previous controller [1]). These results show the advantage of the proposed controller.

4.3. Experiment II: Moving by Hand

Another set of experiments was performed to show the effect of the new position controller in improving the stability of admittance control in physical human-robot interaction. Here, the desired force f_d was set as $f_d = 0$ N. The experimenter grasped the tip of the link and intended to move it sinusoidally at the frequency of approximately 0.5 Hz. The parameters were chosen as $b = 0.1$ Ns/m and $m = 0.05$ kg, which are the same as the case of the foam sheet in Experiment I. In this experiment, the comparison between PDD^2+VFL+FC (the proposed controller) and VPDD^2+FL+FC (the previous controller [1]) are not reported because they produced similar results.

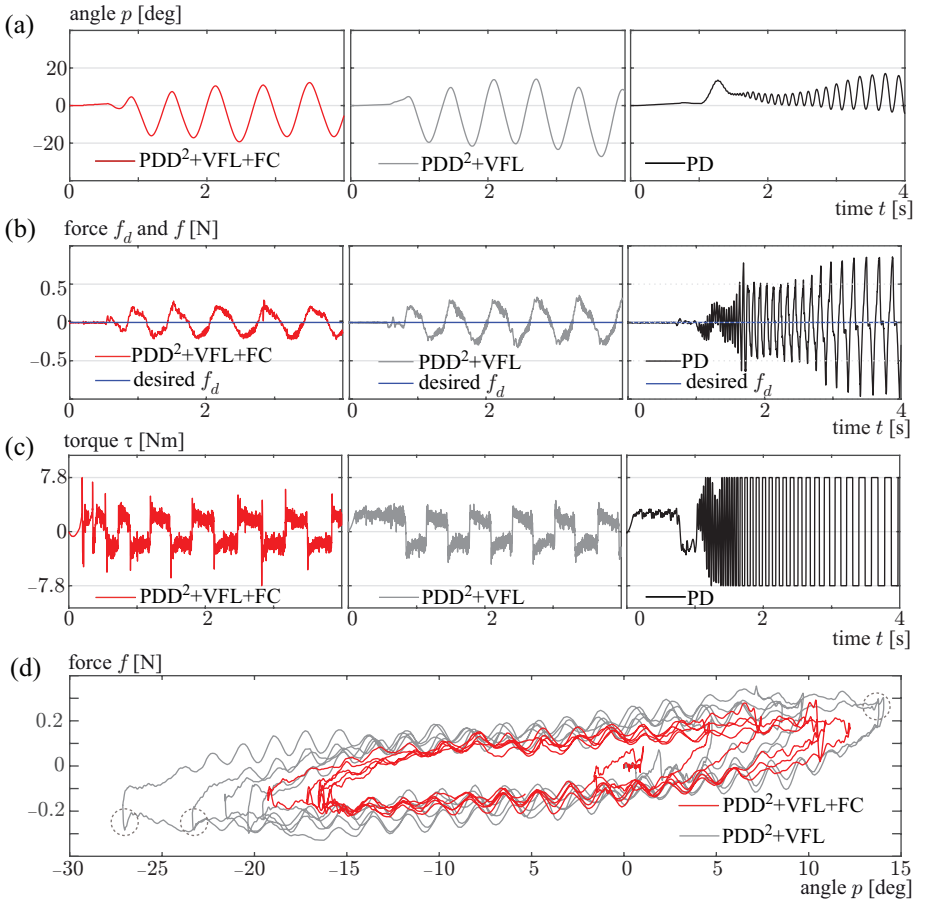

Figure 9: Results of Experiment II: The experimenter intentionally moved the link by hand at the frequency of approximately 0.5 Hz.

Figure 9 shows the results. Here, it must be noted that the operator firmly grasped the link, which produces the destabilizing effect as the high environment stiffness does. As can be seen in Fig. 9(a), it resulted in vibratory, unstable behavior with the PD controller while the intended motion profile was achieved under both PDD^2+VFL+FC (the proposed controller) and PDD^2+VFL (the proposed controller without friction compensation). It is to be noted that the vibration that happened with PD was approximately 10 Hz, which cannot be attributed to the experimenter's voluntary motion but to the controller's in-

stability. The results in Fig. 9(b) indicate that the interaction force is about 0.5 N under both PDD^2+VFL+FC and PDD^2+VFL. Under the conventional PD controller, the oscillatory interaction force with the magnitude of 1 N are resulted regardless of the experimenter's intention to stabilize the system. The controller output signals in Fig. 9(c) reflect the instability under the PD controller because it is saturated almost all the time, which is not the case under either PDD^2+VFL+FC (the proposed controller) or PDD^2+VFL (the proposed controller without friction compensation). These results show that the human-robot interaction may become unstable under the conventional PD controller, and it can be stabilized by incorporating acceleration feedback and friction compensation.

The relation between the angle and interactive force is shown in Fig. 9(d). Here, the results of PD are excluded because it is unstable. It can be observed that inclusion of friction compensation resulted in smaller external force from the experimenter at velocity reversals than the case without friction compensation, as indicated by the dashed grey circles. These results indicate the contribution of friction compensation of the proposed controller.

5. Conclusions

This paper has presented an experimental investigation of a new position controller that is suited as the internal servo of an admittance controller. The new controller consists of three components: (a) PDD^2 position-error feedback, (b) friction compensator [24] and (c) sliding-mode-based filter [25] with a variable gain. The PDD^2 structure and friction compensation are for enhancing the stability of the admittance control. The sliding-mode-based filter is for the mitigation of noise in the acceleration signals without producing a large phase lag. The variable gain of the filter is for suppressing the effect of acceleration-measurement noise at low velocity. The results of several admittance control experiments employing a robotic joint with a force sensor in contact with stiff and soft environments indicate that the proposed position control scheme achieved

an improved stability.

One limitation of the paper is that the new controller was validated only through experiments and formal analysis on the stability is left as an open topic. In particular, switching functions included in both the filter and the friction compensator raise the difficulty that should be addressed in the future study.

References

[1] M. T. S. Aung, R. Kikuuwe, Acceleration feedback and friction compensation for improving the stability of admittance control, In: Proc. Asian Contr. Conf. (2015) 404–409.

[2] S. P. Patarinski, R. G. Botev, Robot force control: A review, Mechatronics 3 (4) (1993) 377 – 398.

[3] D. E. Whitney, Historical perspective and state of the art in robot force control, In: Proc. IEEE Int. Conf. Robot. Autom. 2 (1985) 262–268.

[4] G. Zeng, A. Hemami, An overview of robot force control, Robotica 15 (5) (1997) 473–482.

[5] A. Morbi, M. Ahmadi, A. Chan, R. Langlois, Stability-guaranteed assist-as-needed controller for powered orthoses, IEEE Trans. Control Syst. Technol. 22 (2) (2014) 745–752.

[6] K. Chisholm, K. Klumper, A. Mullins, M. Ahmadi, A task oriented haptic gait rehabilitation robot, Mechatronics 24 (8) (2014) 1083 – 1091.

[7] A. Morbi, M. Ahmadi, Safely rendering small impedances in admittance-controlled haptic devices, IEEE/ASME Transactions on Mechatronics 21 (3) (2016) 1272–1280.

[8] A. Campeau-Lecours, M. Otis, P.-L. Belzile, C. Gosselin, A time-domain vibration observer and controller for physical human-robot interaction, Mechatronics 36 (2016) 45 – 53.

[9] W. Y. Kim, S. Y. Ko, J.-O. Park, S. Park, 6-dof force feedback control of robot-assisted bone fracture reduction system using double f/t sensors and adjustable admittances to protect bones against damage, Mechatronics 35 (2016) 136 – 147.

[10] T. Valency, M. Zacksenhouse, Accuracy/robustness dilemma in impedance control, Trans. ASME J. Dyn. Syst. Meas. Control 125 (3) (2003) 310–319.

[11] S. H. Kang, M. Jin, P. H. Chang, A solution to the accuracy/robustness dilemma in impedance control, IEEE/ASME Trans. Mechatronics 14 (3) (2009) 282–294.

[12] W. S. Newman, Y. Zhang, Stable interaction control and Coulomb friction compensation using natural admittance control, J. Robotic Syst. 11 (1) (1994) 3–11.

[13] M. Dohring, W. Newman, The passivity of natural admittance control implementations, In: Proc. IEEE Int. Conf. Robot. Autom. 3 (2003) 3710–3715.

[14] W. L. Xu, J. D. Han, S. K. Tso, Experimental study of contact transition control incorporating joint acceleration feedback, IEEE/ASME Trans. Mechatronics 5 (3) (2000) 292–301.

[15] W. L. Xu, J. D. Han, S. K. Tso, Y. C. Wang, Contact transition control via joint acceleration feedback, IEEE Trans. Ind. Electron. 47 (1) (2000) 150–158.

[16] R. Kikuuwe, A sliding-mode-like position controller for admittance control with bounded actuator force, IEEE/ASME Trans. Mechatronics 19 (5) (2014) 1489–1500.

[17] G. Aguirre-Ollinger, J. Colgate, M. Peshkin, A. Goswami, Inertia compensation control of a one-degree-of-freedom exoskeleton for lower-limb assistance: Initial experiments, IEEE Trans. Neural Syst. Rehabil. Eng. 20 (1) (2012) 68–77.

[18] V. Duchaine, C. Gosselin, Unified robot control scheme for cooperative motion, autonomous motion and contact reaction, J. Robotics and Mechatronics 23 (4) (2013) 557–566.

[19] K. Hashimoto, Y. Sugahara, H.-O. Lim, A. Takanashi, Biped landing pattern modification method and walking experiments in outdoor environment, J. Robotics and Mechatronics 20 (5) (2013) 775–784.

[20] K. P. Tee, R. Yan, H. Li, Adaptive admittance control of a robot manipulator under task space constraint, In: Proc. IEEE Int. Conf. Robot. Autom. (2010) 5181–5186.

[21] T. Osa, S. Uchida, N. Sugita, M. Mitsuishi, Hybrid rate-admittance control with force reflection for safe teleoperated surgery, IEEE/ASME Trans. Mechatronics 20 (5) (2015) 2379–2390.

[22] F. Dimeas, P. Koustoumpardis, N. Aspragathos, Admittance neuro-control of a lifting device to reduce human effort, Adv. Robotics 27 (12) (2013) 1013–1022.

[23] H. Yu, S. Huang, G. Chen, Y. Pan, Z. Guo, Human-robot interaction control of rehabilitation robots with series elastic actuators, IEEE Trans. Robotics 31 (5) (2015) 1089–1100.

[24] M. T. S. Aung, R. Kikuuwe, M. Yamamoto, Friction compensation of geared actuators with high presliding stiffness, Trans. ASME J. Dyn. Syst. Meas. Control 137 (1) (2015) 011007.

[25] M. T. S. Aung, Z. Shi, R. Kikuuwe, A new noise reduction filter with sliding mode and low-pass filtering, In: Proc. IEEE Conf. Contr. Appl. (2014) 1029–1034.

[26] R. Kikuuwe, K. Kanaoka, T. Kumon, M. Yamamoto, Phase-lead stabilization of force-projecting master-slave systems with a new sliding mode filter, IEEE Trans. Control Syst. Technol. 23 (6) (2015) 2182–2194.

[27] M. T. S. Aung, R. Kikuuwe, Acceleration feedback and friction compensation for improving positioning performance in systems with friction, In: Proc. American Contr. Conf. (2015) 4798–4803.

[28] S. Jin, R. Kikuuwe, M. Yamamoto, Parameter selection guidelines for a parabolic sliding mode filter based on frequency and time domain characteristics, J. Control Sci. Eng. 2012 (2012) 923679.

[29] S. Jin, R. Kikuuwe, M. Yamamoto, Real-time quadratic sliding mode filter for removing noise, Adv. Robotics 26 (8-9) (2012) 877–896.